Understanding Transport Mechanisms in Ionic Liquid/Carbonate Solvent Electrolyte Blends

K. Oldiges,[a,b] D. Diddens,[a] M. Ebrahiminia,[c] J. B. Hooper,[c] I. Cekic-Laskovic,[a,b,d] A. Heuer,[a,b] D. Bedrov,*[c] M. Winter,[a,b,d] and G. Brunklaus*[a,b,d]

d.bedrov@utah.edu , g.brunklaus@fz-juelich.de

a. Helmholtz Institute Münster, IEK-12, Forschungszentrum Jülich GmbH, Corrensstrasse 46, 48149 Münster, Germany

b. Institute of Physical Chemistry, University of Münster, Corrensstrasse 28/30, 48149 Münster, Germany

c. Department of Materials Science & Engineering, University of Utah, 122 South Central Campus Drive, Salt Lake City, Utah 84112, USA

d. MEET Battery Research Center, Corrensstrasse 46, 48149 Münster, Germany

SUPPLEMENTARY INFORMATION

Raman spectra

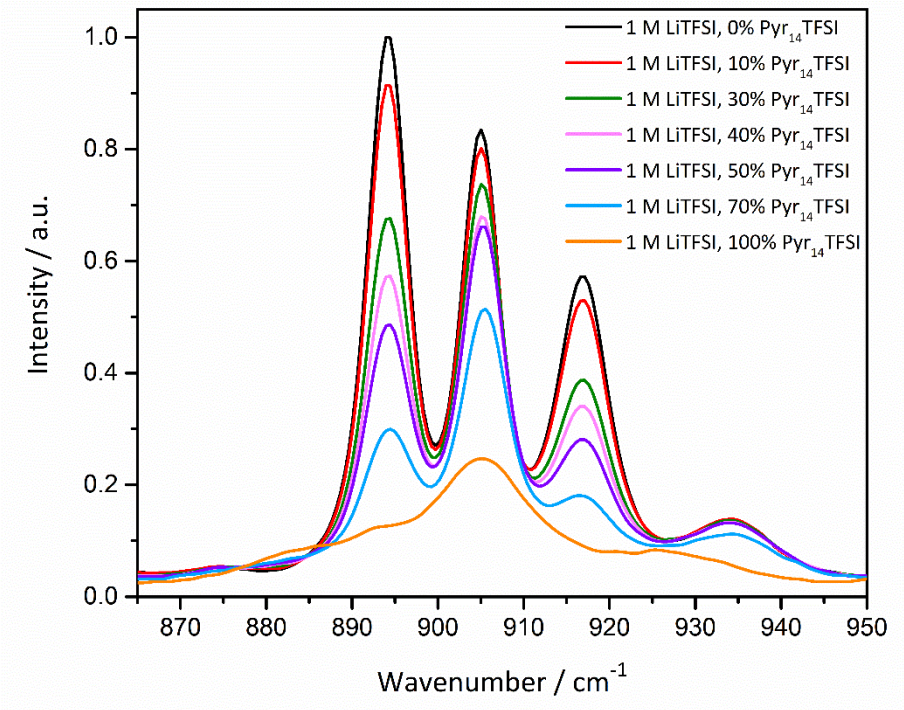

Figure S1. Raman spectra of investigated $Pyr_{14}TFSI$/EC/DMC blends with 1 M LiTFSI as conducting salt in the range from 865 to 950 cm^{-1}.

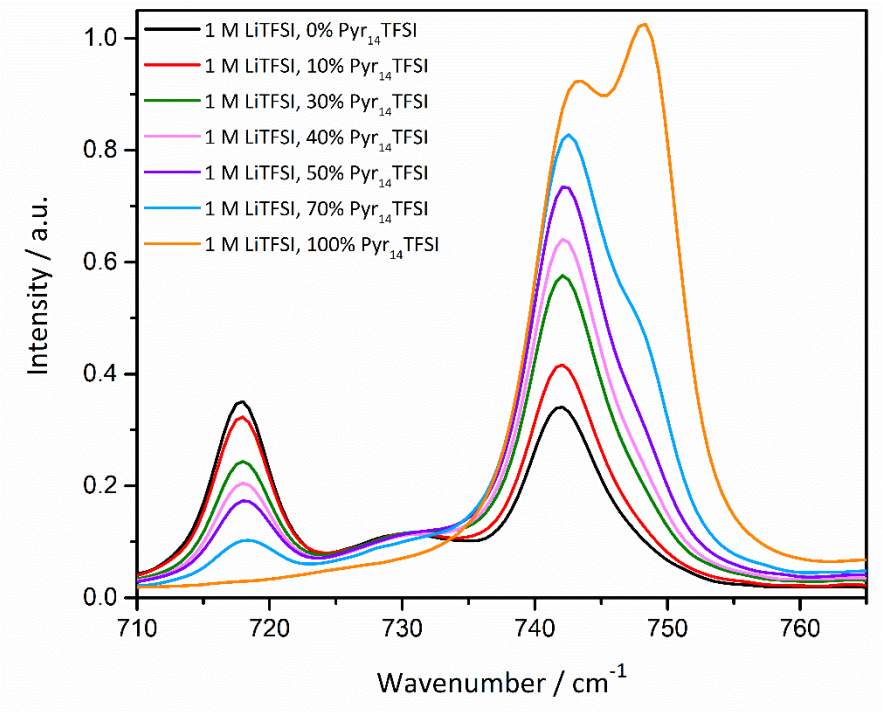

Figure S2. Raman spectra of investigated $Pyr_{14}TFSI$/EC/DMC blends with 1 M LiTFSI as conducting salt in the range from 710 to 765 cm^{-1}.

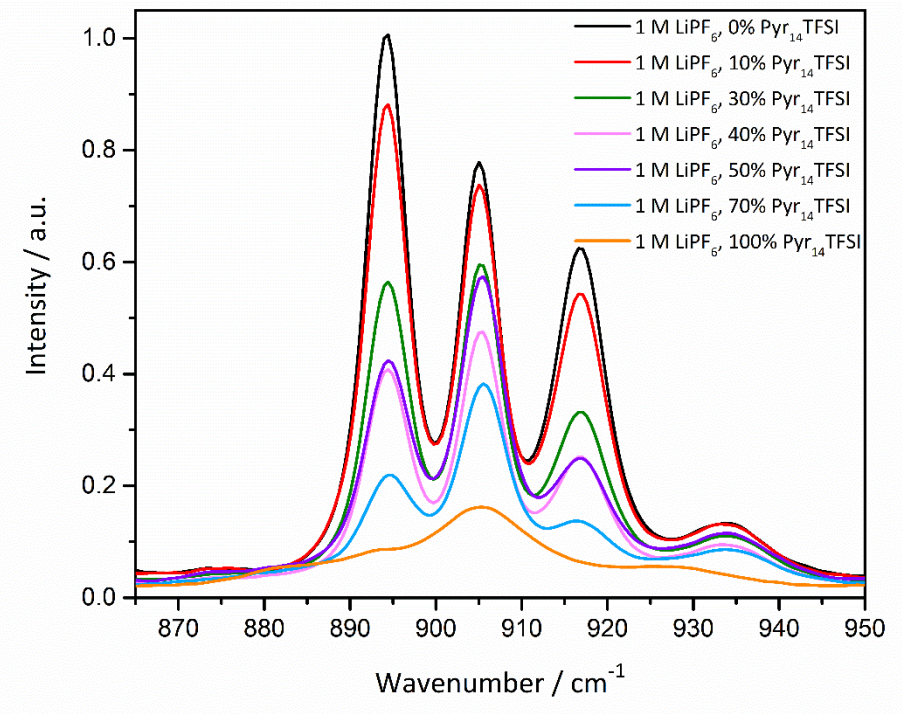

Figure S3. Raman spectra of investigated $Pyr_{14}TFSI$/EC/DMC blends with 1 M $LiPF_6$ as conducting salt in the range from 865 to 950 cm^{-1}.

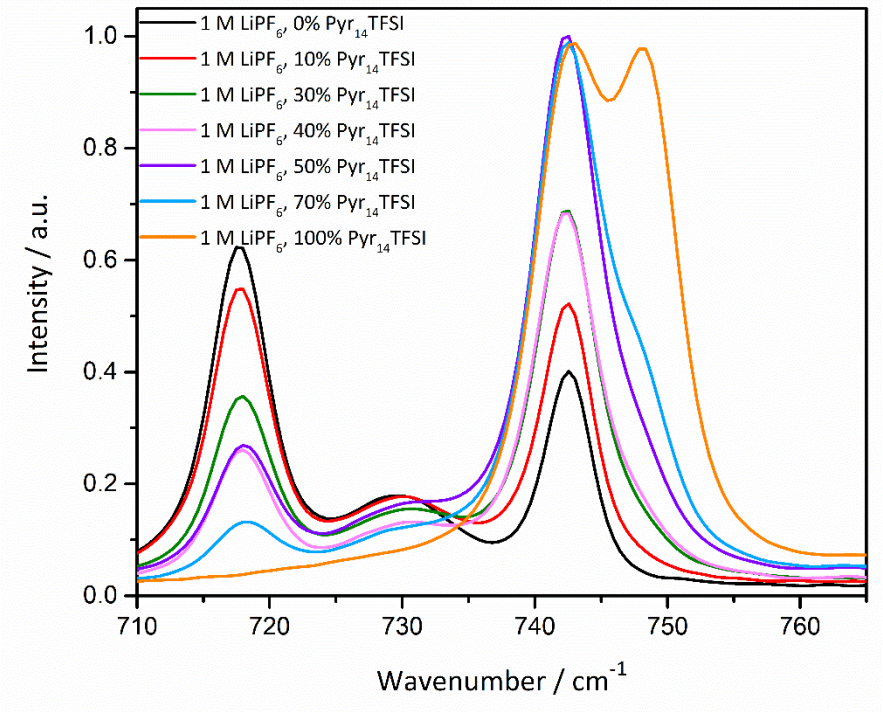

Figure S4. Raman spectra of investigated $Pyr_{14}TFSI$/EC/DMC blends with 1 M $LiPF_6$ as conducting salt in the range from 710 to 765 cm^{-1}.

Radial Distribution Function

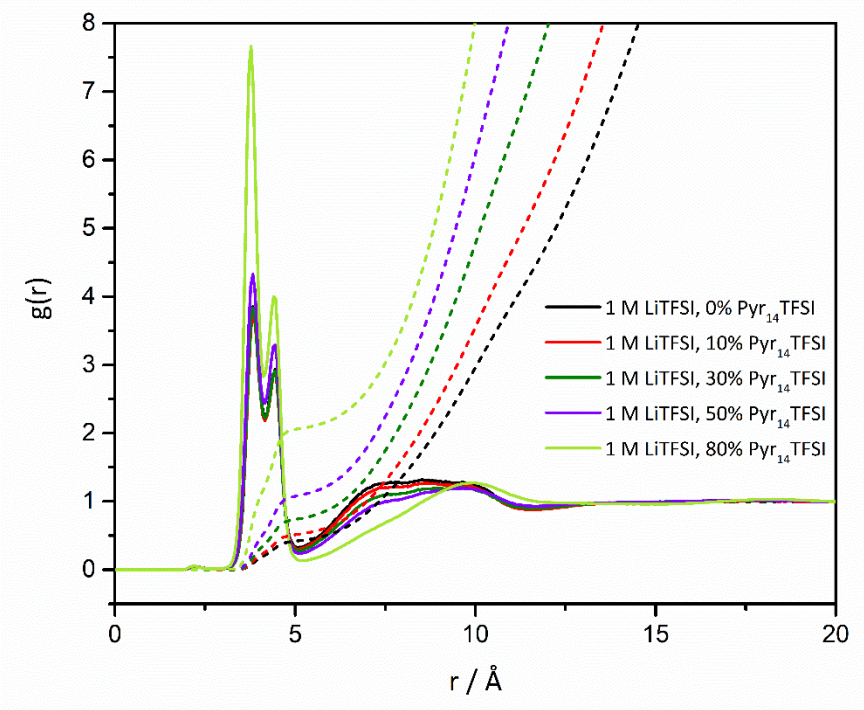

Figure S5. Radial distribution functions (RDFs) between Li^+ ions and the nitrogen atoms of TFSI for different fractions of $Pyr_{14}TFSI$. The dashed lines correspond to the integrated curves, from which the coordination numbers have been extracted at 4.16 Å for the population of bidentate coordinations and at 5.0 Å for the sum of mono- and bidentate coordinations.

Self-diffusion coefficients

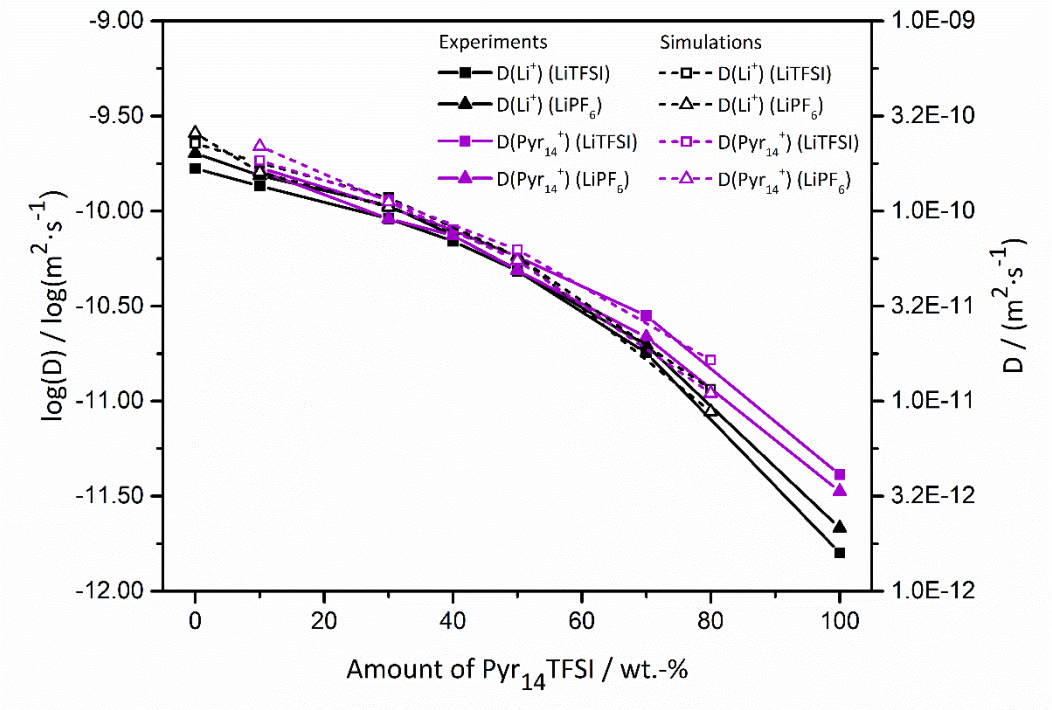

Figure S6. Self-diffusion coefficients of all cationic species present in blends of $Pyr_{14}TFSI$, EC and DMC with 1 M LiTFSI and 1 M $LiPF_6$ as conducting salts at 25°C. ■▲ Experimental data points. □△ Simulation data points. The solid and dashed lines are guides to the eye.

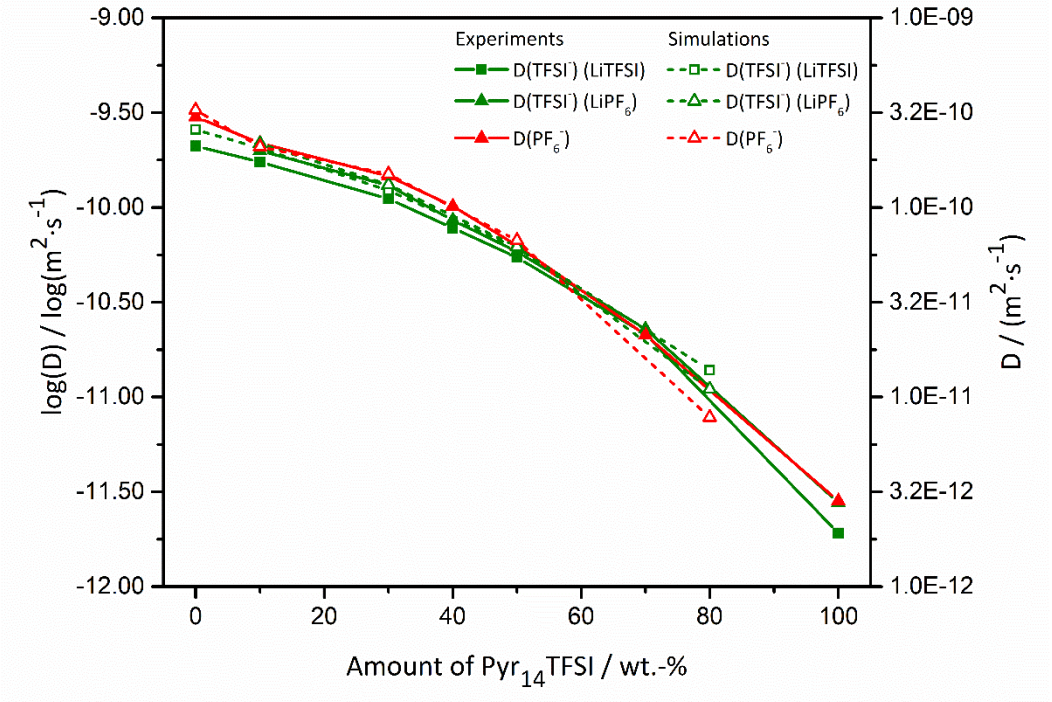

Figure S7. Self-diffusion coefficients of all anionic species present in blends of $Pyr_{14}TFSI$, EC and DMC with 1 M LiTFSI and 1 M $LiPF_6$ as conducting salts at 25°C. ■▲ Experimental data points. □△ Simulation data points. The solid and dashed lines are guides to the eye.

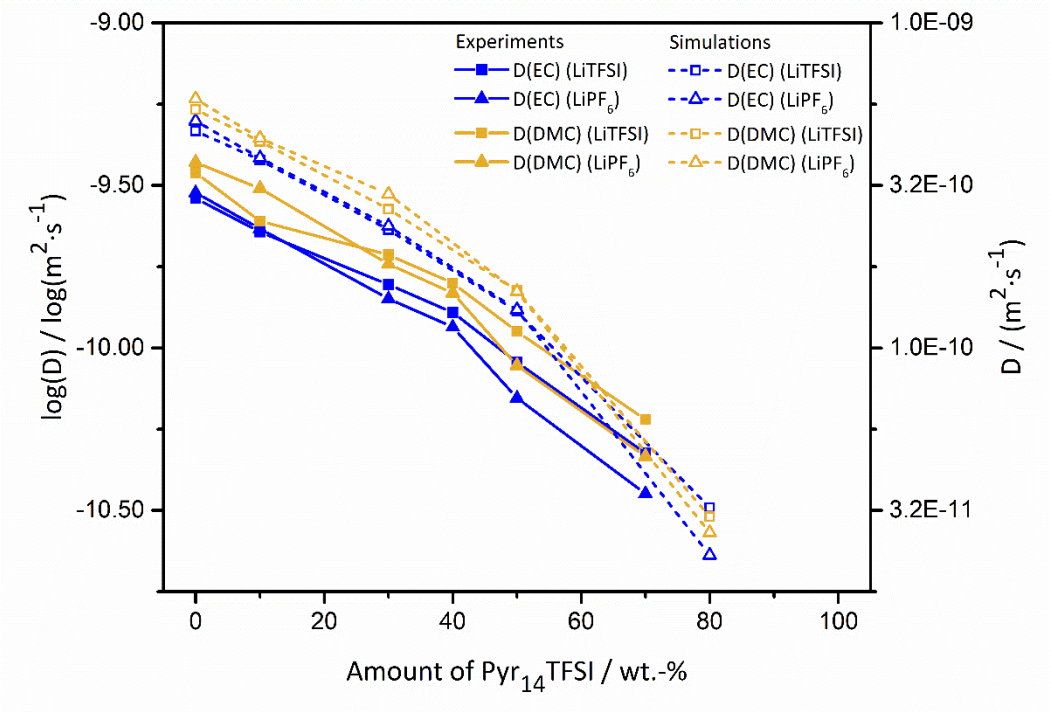

Figure S8. Self-diffusion coefficients of all neutral species present in blends of $Pyr_{14}TFSI$, EC and DMC with 1 M LiTFSI and 1 M $LiPF_6$ as conducting salts at 25°C. ■▲ Experimental data points. □△ Simulation data points. The solid and dashed lines are guides to the eye.

Impedance measurements

Cell design and calibration

The cells comprise coaxial impedance electrodes of stainless steel with an outer diameter of 6 mm. The outer ring electrode and the PEEK isolator have thicknesses of 1 mm and 1.5 mm, respectively. The electrode in the middle has a diameter of 1 mm. The cell was calibrated with a 0.01 M KCl solution as conductance standard according to ISO 7888 (Sigma-Aldrich).

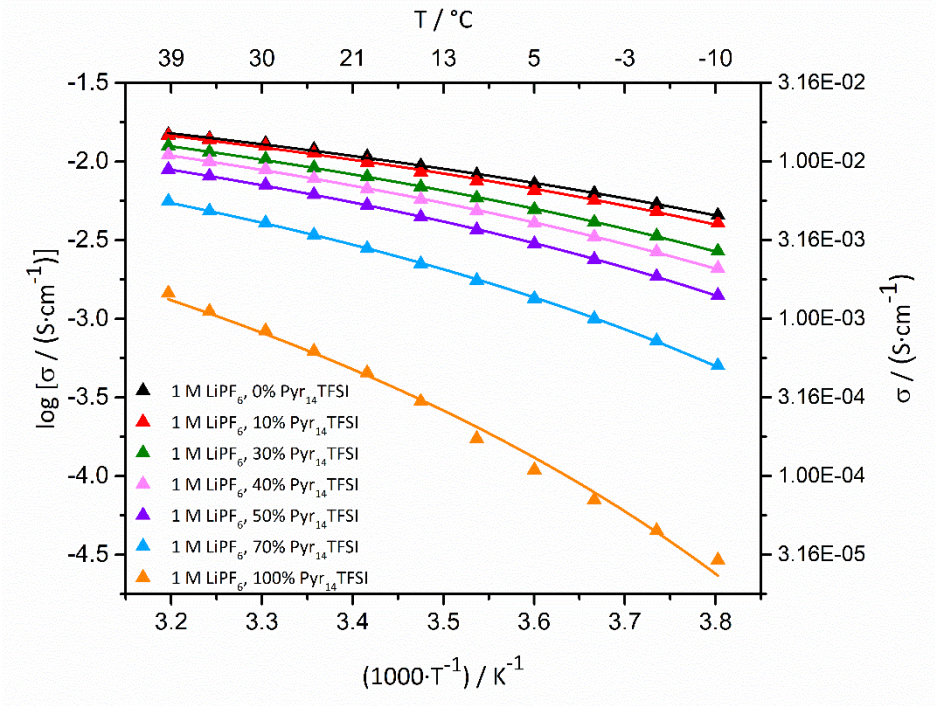

Figure S9. Arrhenius plot of ionic conductivities of $Pyr_{14}TFSI$/EC/DMC blends with 1 M $LiPF_6$ as conducting salt measured from -10 to 40 °C using impedance. The data points are fitted using VTF function.

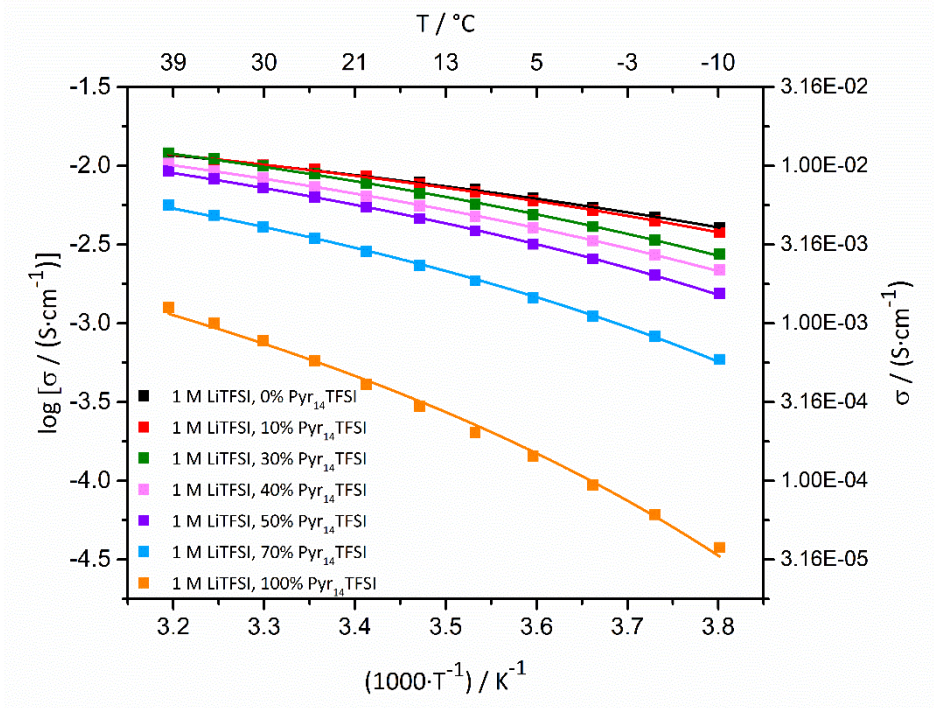

Figure S10. Arrhenius plot of ionic conductivities of $Pyr_{14}TFSI$/EC/DMC blends with 1 M LiTFSI as conducting salt measured from -10 to 40 °C using impedance. The data points are fitted using VTF function.

Viscosities

Experimental

Viscosity measurements were performed with an Anton Paar MCR 301 rheometer in a dry room (water content below 30 ppm). The device was equipped with a temperature system CTD 450 and a CP50-0.5/TG measuring system with a diameter of 49.947 mm, a cone angle of 0.473° and a distance of 68 µm between cone and lower plate. The viscosities were measured in a temperature range of -10 °C to 40 °C in steps of 10 °C; viscosities were also measured at 25 °C. The shear rates were increased with increasing temperature from 800 s^{-1} to 2800 s^{-1}.

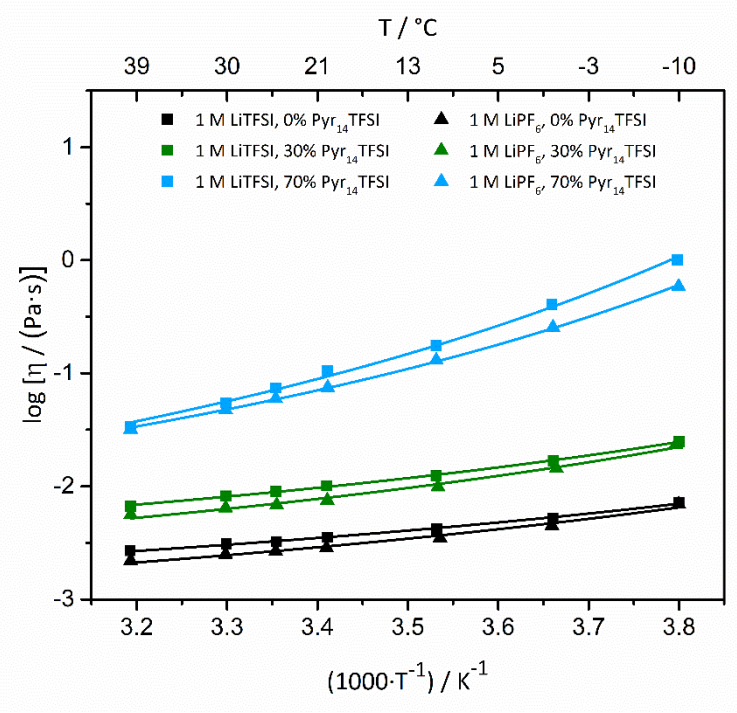

Figure S11. Arrhenius plot of viscosities of $Pyr_{14}TFSI$/EC/DMC blends (0, 30 and 70% $Pyr_{14}TFSI$) with 1 M LiTFSI and 1 M $LiPF_6$ as conducting salts measured from -10 to 40 °C. The data points are fitted using VTF functions.

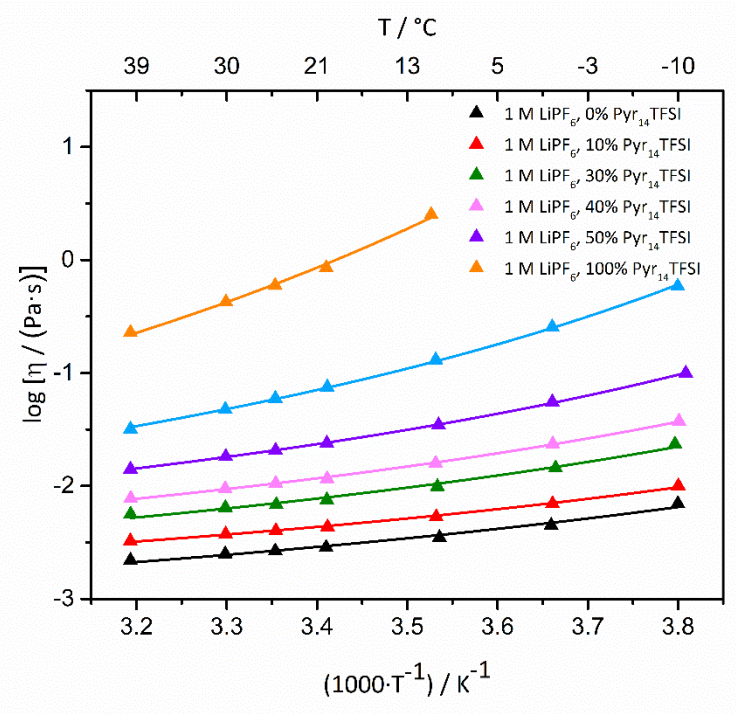

Figure S12. Arrhenius plot of viscosities of $Pyr_{14}TFSI$/EC/DMC blends with 1 M $LiPF_6$ as conducting salt measured from -10 to 40 °C. The data points are fitted using VTF functions. The viscosities of solutions containing 100% $Pyr_{14}TFSI$ could not be measured at low temperatures due to partial solidification.

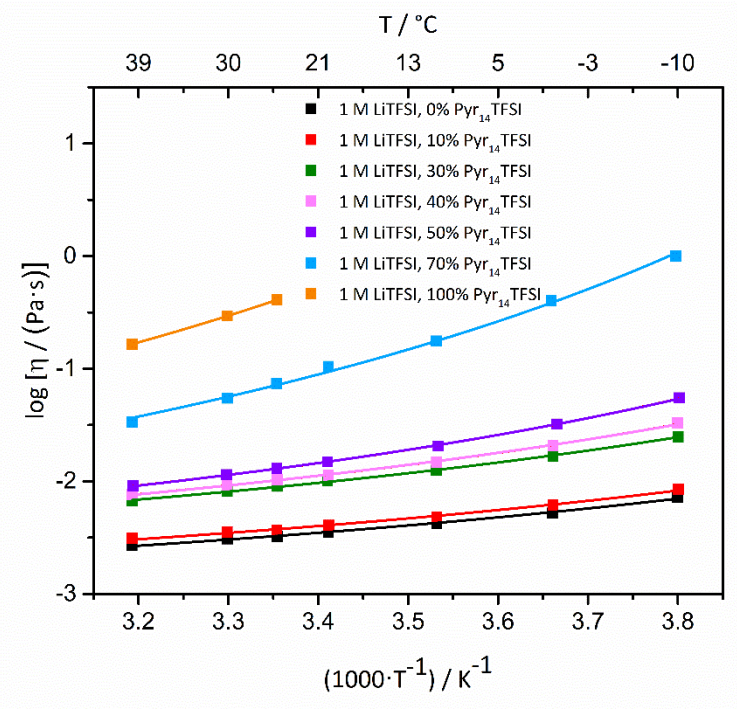

Figure S13. Arrhenius plot of viscosities of $Pyr_{14}TFSI$/EC/DMC blends with 1 M LiTFSI as conducting salt measured from -10 to 40 °C. The data points are fitted using VTF functions. The viscosities of solutions containing 100% $Pyr_{14}TFSI$ could not be measured at low temperatures due to partial solidification.

Degree of ion dissociation

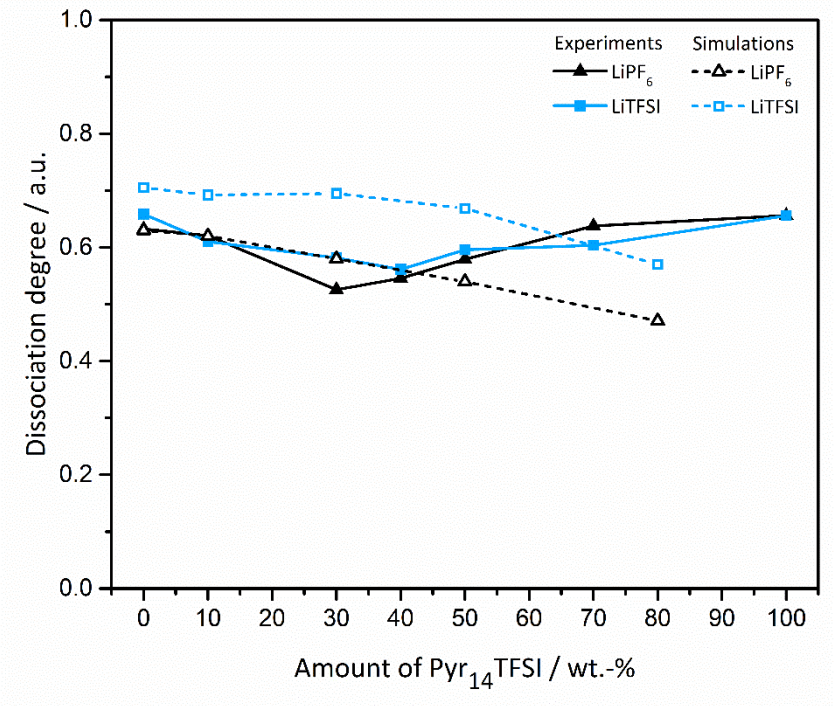

Figure S14. Dissociation degree of the conducting salts LiTFSI and $LiPF_6$ in blends of $Pyr_{14}TFSI$, EC and DMC at 25 °C. ■▲ Experimental data points. □△ Simulation data points. The solid and dashed lines are guides to the eye.

Thermal stability

Experimental

Thermal gravimetric analysis (TGA)

Thermal gravimetric analysis (TGA) measurements were performed with a TGA Q5000 measuring device. The samples were prepared in sealed aluminum pans, which were tared before use. After an equilibration at 30 °C and an isothermal step for 10 minutes, the temperature was raised up to 575 °C with 10 °C per minute and the weights of the samples were measured. Nitrogen was used as balance and sample gas.

Differential scanning calorimetry (DSC)

Differential scanning calorimetry (DSC) measurements were performed with a DSC Q2000 measuring device. The samples were prepared in hermetic aluminum pans. After an equilibration at 40 °C and an isothermal step for two minutes, heat flow was measured three times from 40 °C to -150 °C to again 40 °C. Helium and nitrogen were both used as ambient gases with 25 ml/min.

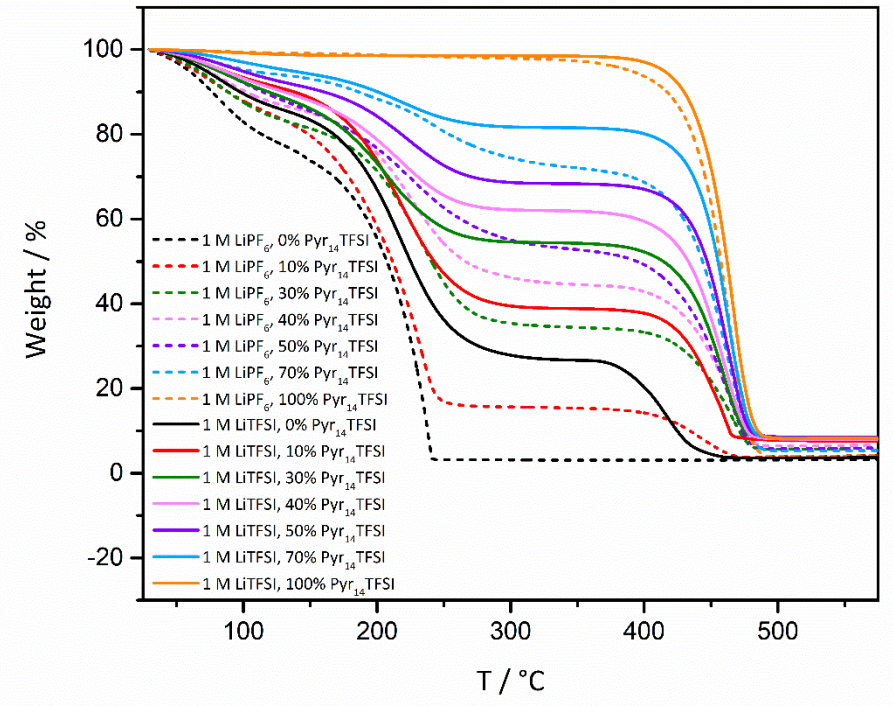

Figure S15. Weight loss in % of the investigated $Pyr_{14}TFSI$/EC/DMC samples with increasing temperature (30 - 575 °C) resulting from TGA measurements.

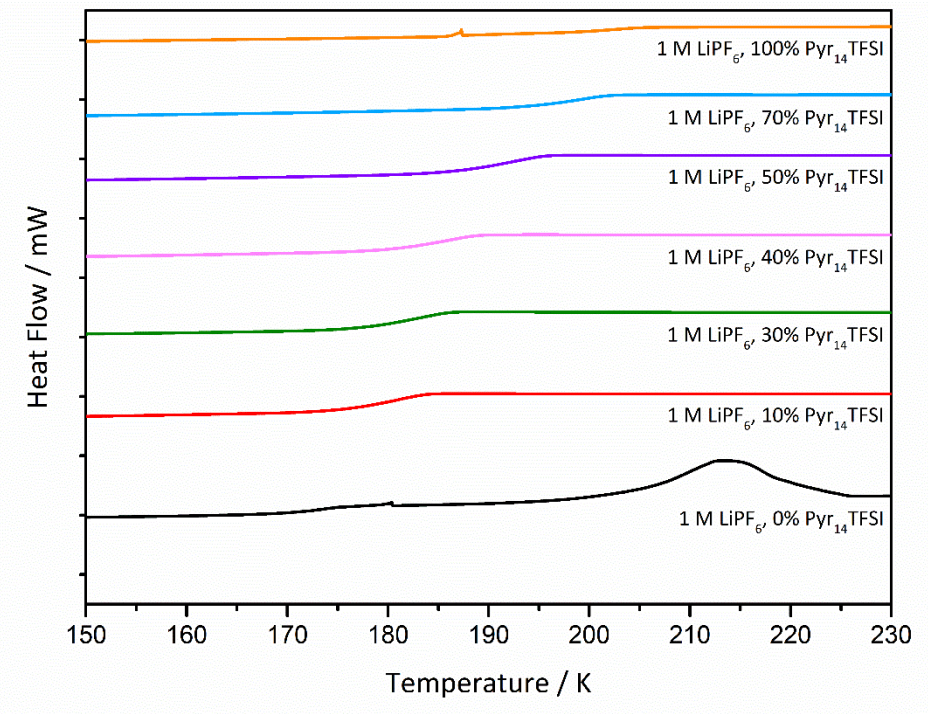

Figure S16. Heat flows in mW in the temperature range from 150 to 230 K for blends of 1 M $LiPF_6$ in $Pyr_{14}TFSI$/EC/DMC resulting from DSC measurements.

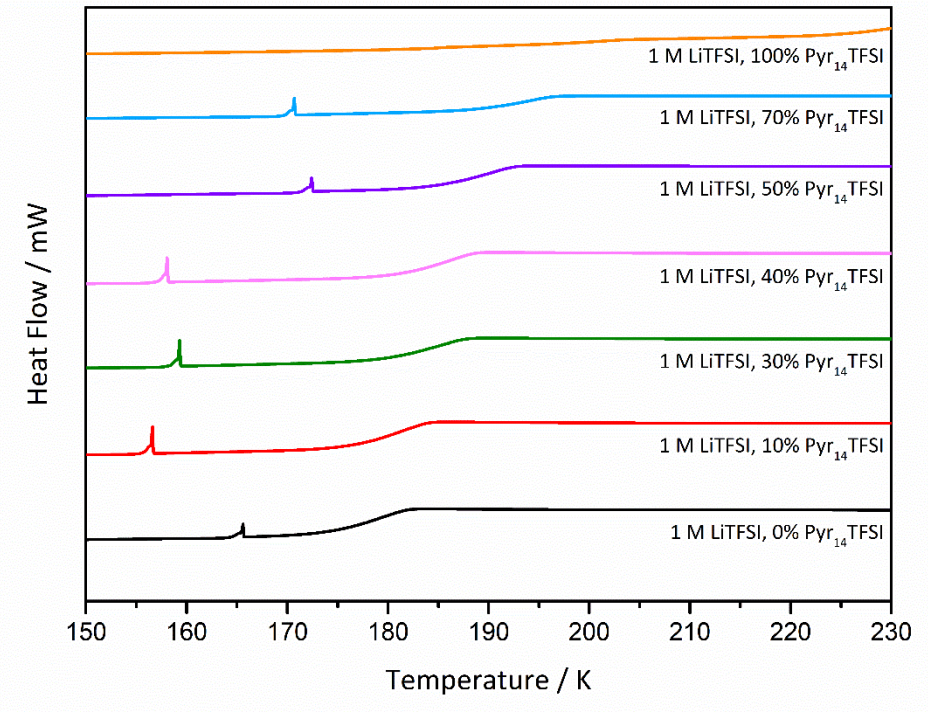

Figure S17. Heat flows in mW in the temperature range from 150 to 230 K for blends of 1 M LiTFSI in $Pyr_{14}TFSI$/EC/DMC resulting from DSC measurements.

Table ST1. VTF activation energies derived from fitting viscosity and impedance data and glass transition temperatures of $Pyr_{14}TFSI$/EC/DMC blends with 1 M $LiPF_6$ and 1 M LiTFSI as conducting salts.

	Amount of $Pyr_{14}TFSI$ / wt-%	**T_g / K**	**B_{Visco} / K**	**B_{Imp}/ K**	**B_{Visco}·R / kJ·mol^{-1}**	**B_{Imp}·R / kJ·mol^{-1}**
1 M $LiPF_6$	0	175 ±4	120 ±9	128 ±9	1.00 ±0.07	1.06 ±0.07
	10	182 ±4	103 ±8	121 ±9	0.86 ±0.07	1.01 ±0.07
	30	185 ±4	127 ±11	135 ±11	1.06 ±0.09	1.12 ±0.09
	40	187 ±3	132 ±8	139 ±8	1.10 ±0.07	1.16 ±0.07
	50	192 ±2	144 ±6	139 ±6	1.20 ±0.05	1.16 ±0.05
	70	196 ±2	180 ±9	164 ±7	1.50 ±0.07	1.36 ±0.06
	100	198 ±1	345 ±8	263 ±6	2.87 ±0.10	2.19 ±0.08
1 M LiTFSI	0	176 ±3	101 ±6	110 ±7	0.84 ±0.06	0.91 ±0.07
	10	179 ±2	99 ±3	112 ±5	0.82 ±0.04	0.93 ±0.05
	30	184 ±2	114 ±4	133 ±5	0.95 ±0.04	1.11 ±0.04
	40	185 ±1	126 ±5	136 ±5	1.05 ±0.05	1.13 ±0.06
	50	191 ±2	137 ±6	137 ±6	1.14 ±0.06	1.14 ±0.06
	70	195 ±2	169 ±8	158 ±7	1.41 ±0.08	1.31 ±0.07
	100	198 ±0	301 ±6	231 ±5	2.50 ±0.08	1.92 ±0.06

Electrochemical stability

Experimental

Linear sweep voltammetry (LSV)

In order to determine the electrochemical stability window (ESW), linear sweep voltammetry (LSV) measurements were performed with a VMP3 (BioLogic Science Instruments) from 0 to 6 V with a scan rate of 0.1 mV s^{-1}. A three-electrode Swagelok cell was used with platinum (Ø 1 mm) as working electrode and lithium metal as counter (Ø 12 mm) and reference (Ø 5 mm) electrode. Freudenberg FS 2190 was used as separator. The measurements were performed at room temperature.

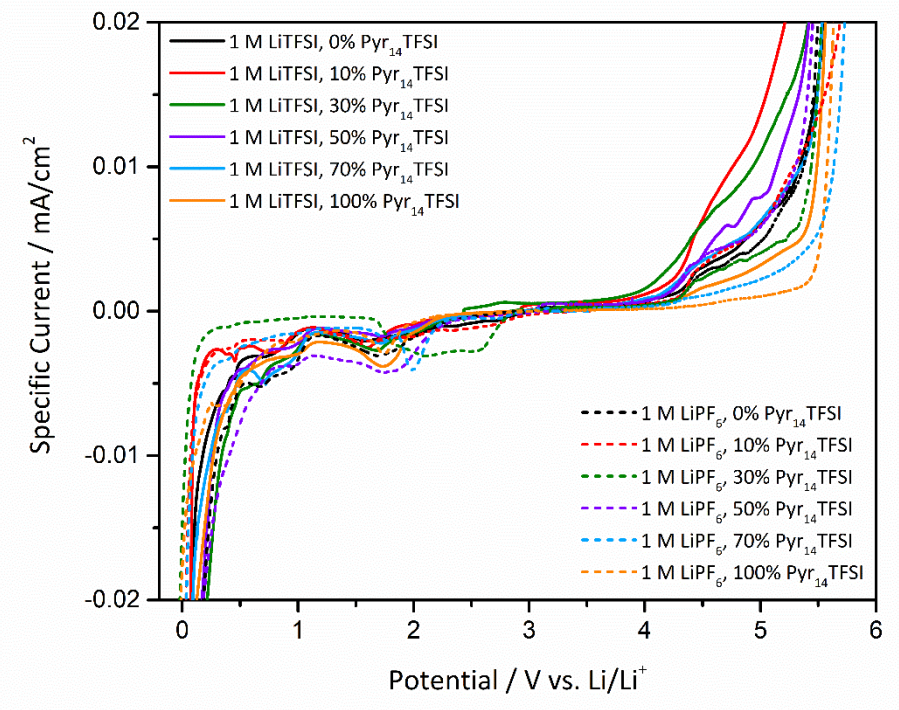

Figure 18. Linear sweep voltammetry profiles of the investigated $Pyr_{14}TFSI$/EC/DMC blends with 1 M $LiPF_6$ and 1 M LiTFSI as conducting salts at room temperature with a scan rate of 0.1 mV/s.